N. Miner. Abh. (J. Min. Geochem.)
Published online March 2018

PrePub Article

Sulfur isotope geochemistry of the Chodarchay Cu-Au deposit, Tarom, NW Iran

Narges Yasami, Majid Ghaderi, Pura Alfonso

With 10 figures and 1 table

Abstract: The Chodarchay porphyry–high-sulfidation epithermal Cu-Au deposit in the Tarom subzone of the western Alborz structural zone of NW Iran is related to quartz-monzonite and alkali-granite intrusions that were emplaced within the volcanic-volcaniclastic rocks of Karaj Formation during Tertiary. The Chodarchay deposit formed as a high-sulfidation epithermal overprint on porphyry type mineralization. The mineralization occurred as stockwork, dissemination, veinlet, open space filling and breccias. Chalcopyrite, pyrite, sphalerite, and galena are the main sulfide minerals in the area. The sulfur isotope composition of sulfide minerals from the Chodarchay deposit is positive, ranging from 0.2 to 6.8 ‰. The sphalerite-galena isotope geothermometer shows 360 °C for the crystallization temperature. Sulfur was sourced from a homogeneous magma, and its isotopic composition decreases with depth and temperature decreasing due to fluid oxidation changes. Therefore, sulfur isotope assemblages show a systematic spatial distribution within the Chodarchay system.

Key words: Porphyry–epithermal, sulfur isotopes, magmatic source, Chodarchay, Tarom, Iran.

1. Introduction

Stable isotopes have been studied for decades on precious metal deposits (Simmons et al. 2005, Taylor 2007). Sulfur isotope characteristics of sulfides and sulfates provide valuable information on the genesis of porphyry copper deposits (PCDs) (e.g. Field et al. 2005, Rye 2005, John et al. 2010, Qiu et al. 2016). Although PCDs usually present $\delta^{34}S$ sulfide values near 0 ‰ (Ohmoto & Rye 1979) that is indicative of their close magmatic origin, these deposits can be identified by a wide range of $\delta^{34}S$ values (John 2010).

A number of studies have recorded the sulfur stable isotope composition of Tarom metallogenic subzone of NW Iran. Taghipour & Mackizadeh (2010) used sulfur stable isotope geochemistry on alunite to determine hydrothermal alteration in Takestan, Tarom subzone, and attributed a magmatic origin of alteration fluids although the $\delta^{34}S$ values of sulfate from alunite were relatively high (13.9–18.1 ‰) . Advanced argillic alteration has been detected through stable isotope studies in the Tarom subzone by Hashemi & Taghipour (2010). Sulfur stable isotopes have also been studied in the Khalyfehlou volcanic-hosted vein-type copper deposit, Tarom. The sulfur isotope values for the chalcopyrite range from −2.0 to −5.3 ‰. The occurrence of framboidal pyrite in the tuffaceous sandstone host rocks and negative sulfur isotope values suggest a sedimentary origin for the sulfur (Esmaeli et al. 2015).

The aim of this research is to study sulfur stable isotopes for understanding ore-forming processes at the Chodarchay porphyry-epithermal Cu-Au deposit, which is related to the northern magmatism on the western part of Tarom. In this contribution, we report results obtained from sulfur isotope studies for the deposit. The Chodarchay sulfur isotope composition has been compared with southern intrusion-related deposits like Khalyfehlou, where mineralization shows similarities with Cordilleran vein-type deposits (Esmaeli et al. 2015).

2. Regional geology

The Chodarchay deposit is a part of the Tarom subzone, western Alborz belt of northwestern Iran approximately 50 km east of the city of Zanjan. The Alborz magmatic belt with an E–W orientation 600 km in length and 100 km in width situated in northern Iran and the Tabriz Fault,

DOI: 10.1127/njma/2018/0097

www.schweizerbart.de
0077-7757/2018/0097 $ 0.00

has separated it from the Central Iranian microplate in the south; the belt extends into Armenia to the north (Azizi & Jahangiri 2008). The N–S trending Rasht-Takestan Fault has divided this belt into western and eastern parts. The calc-alkaline Eocene andesitic to dacitic lava and many granitoids constitute the western part (Moayyed 2001, Nabatian & Ghaderi 2013, Nabatian et al. 2013). These calc-alkaline and alkaline volcanic and plutonic rocks formed within an extensional (post-collisional) environment in the arc and back-arc settings (Berberian 1983, Hassanzadeh et al. 2002, Allen et al. 2003, Mirnejad et al. 2010). Cenozoic marine and subaerial successions of the Alborz magmatic belt include porphyritic and non-porphyritic, massive lava flows that range in composition from andesite, basaltic andesite to basalt (Aghazadeh et al. 2010). Cenozoic strata in the northwestern part of the Alborz magmatic belt were intruded by post-collisional magmatic-related shoshonitic and high-K calc-alkaline Upper Eocene and Oligo-Miocene plutons (Berberian & King 1981, Aghazadeh et al. 2010, Verdel et al. 2011, Nabatian & Ghaderi 2013, Nabatian et al. 2013, 2014).

Magmatism in the Tarom volcano-plutonic complex began during the Eocene and continued throughout the late Eocene. This region is mostly composed of pyroclastic rocks (Karaj Formation) followed by late Eocene-post Eocene plutonic rocks (Fig. 1). The Eocene calc-alkaline to alkaline marine volcanism along the Tarom is marked by pyroclastic and lava flows of trachyte, trachy-andesite, andesite, basaltic andesite, olivine-basalt, porphyritic and non-porphyritic rhyodacite (Bolourian 1994, Moayyed 2001, Nabatian 2011). Sedimentary rocks such as limestone and sandstone at the base accompany this period of intense volcanic activity. The 20–25 km elongated NW–SE trending Tarom plutonic complex is widespread throughout the Tarom subzone (Nabatian et al. 2014). The Tarom region includes porphyry, epithermal, iron oxide apatite, sediment-hosted copper deposits and intrusion-related vein systems (e.g. Nabatian et al. 2013, Mehrabi et al. 2016, Mokhtari et al. 2016, Yasami et al. 2017). Several epithermal deposits are known from the Tarom belt, in the vicinity of the Chodarchay deposit (Esmaeli et al. 2015, Zamanian et al. 2015, Hosseinzadeh et al. 2016).

3. The Chodarchay deposit geology

The Chodarchay deposit is located in the western part of the Tarom volcano-plutonic belt. The deposit is hosted by Eocene volcanic-volcaniclastic rocks and late Eocene-post Eocene stock. Local Oligocene tuff crops out to the north of the deposit. The Eocene volcanic and volcaniclastic rocks (Karaj Formation) overlie most parts of the Chodarchay area.

Porphyry-epithermal style mineralization at the Chodarchay is within the mineralized quartz monzonite stock and their host rocks. Alteration types extend vertically and laterally from the porphyry mineralization. The inner potassic zone is surrounded by phyllic, argillic and peripheral propylitic alteration assemblages. Structurally-controlled alteration and mineralization occurs along the NW-striking fault in the deposit (Yasami et al. 2017).

Detailed field observations and core logging has identified intrusive rocks to include quartz monzonite to alkali-granite series and late alkali-granite stock (Fig. 2a–e). The ore-hosting quartz monzonite series (Fig. 2f) is exposed in the southeastern part of the deposit and is cut by later alkali-granites. The second stock is exposed to the north of the quartz monzonite stock. Emplacement of these two intrusion types was controlled by the NW-striking fault.

4. Methods and materials

4.1. Field mapping

Fieldwork was carried out over a few visits to the Chodarchay district. Total field activity included mapping of excavated faces and logging of diamond drill cores. Field relationships among the different magmatic units are studied. Mapping of the local geology in the mine area was carried out concurrently during field surveys with sampling for ore petrography and geochemical analysis from outcrop and drill cores. A total of 352 surface samples and also core samples from various depths were collected for laboratory analyses.

4.2. Ore petrography

The development of mineralization in the Chodarchay deposit was determined by detailed macroscopic to microscopic ore petrography. The characteristics of each sample were determined using petrography. 130 suitable specimens were chosen. Seventy thin, 50 thin-polished and 10 thick-polished sections were prepared and then examined by reflected light microscopy. Ore petrography was conducted at the Tarbiat Modares University, using a standard microscope. Based on various sulfide ore minerals, contemporaneous association, and different depths, eighteen of the studied key samples were selected for the sulfur isotope study.

4.3. Sulfur isotope analysis

Sulfur isotope measurements were made on sulfide minerals separated from 18 rock samples (Table 1). Samples

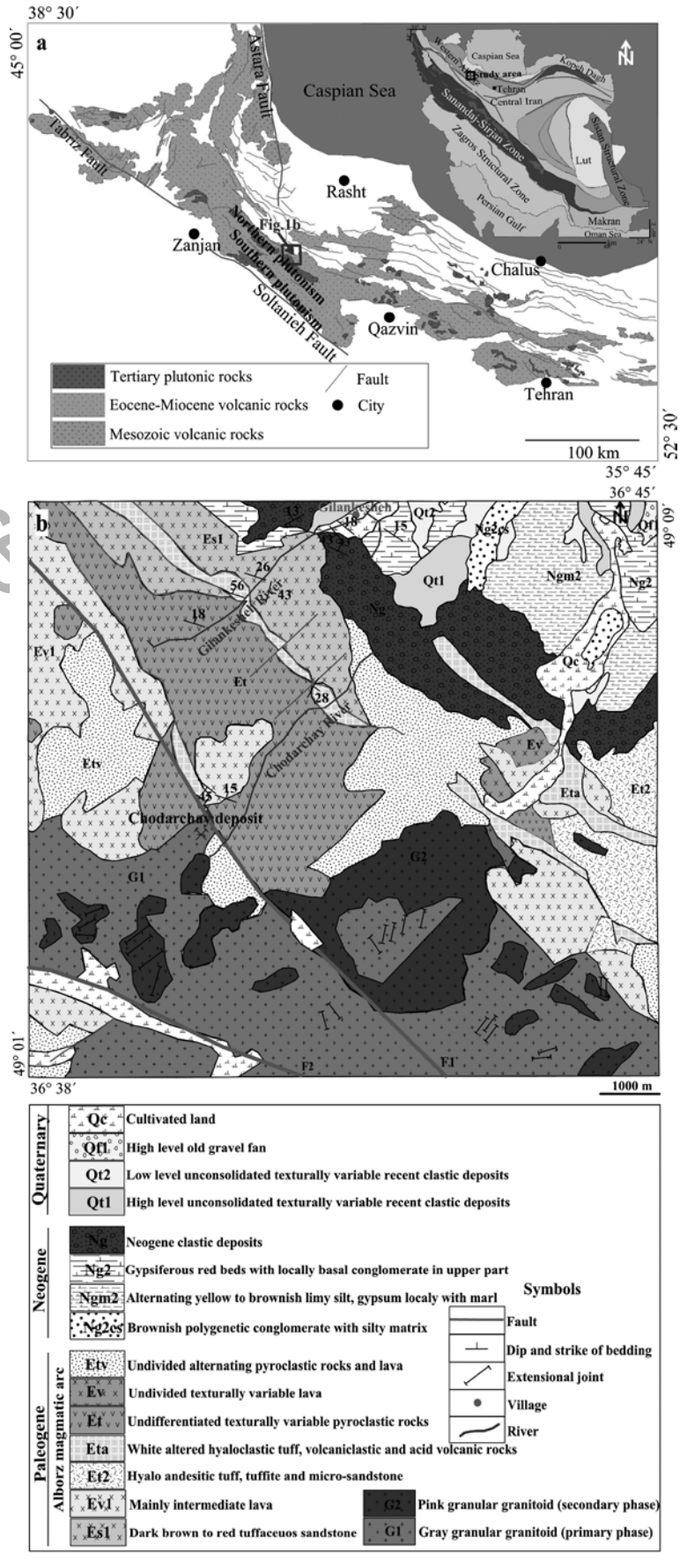

Fig. 1. Geological map of the study area revised and modified based on the new field data from 1:100,000 geological map of Roudbar (modified after Nazari & Salamati 1998). Star marks the location of the Chodarchay deposit (modified after Yasami et al. 2017).

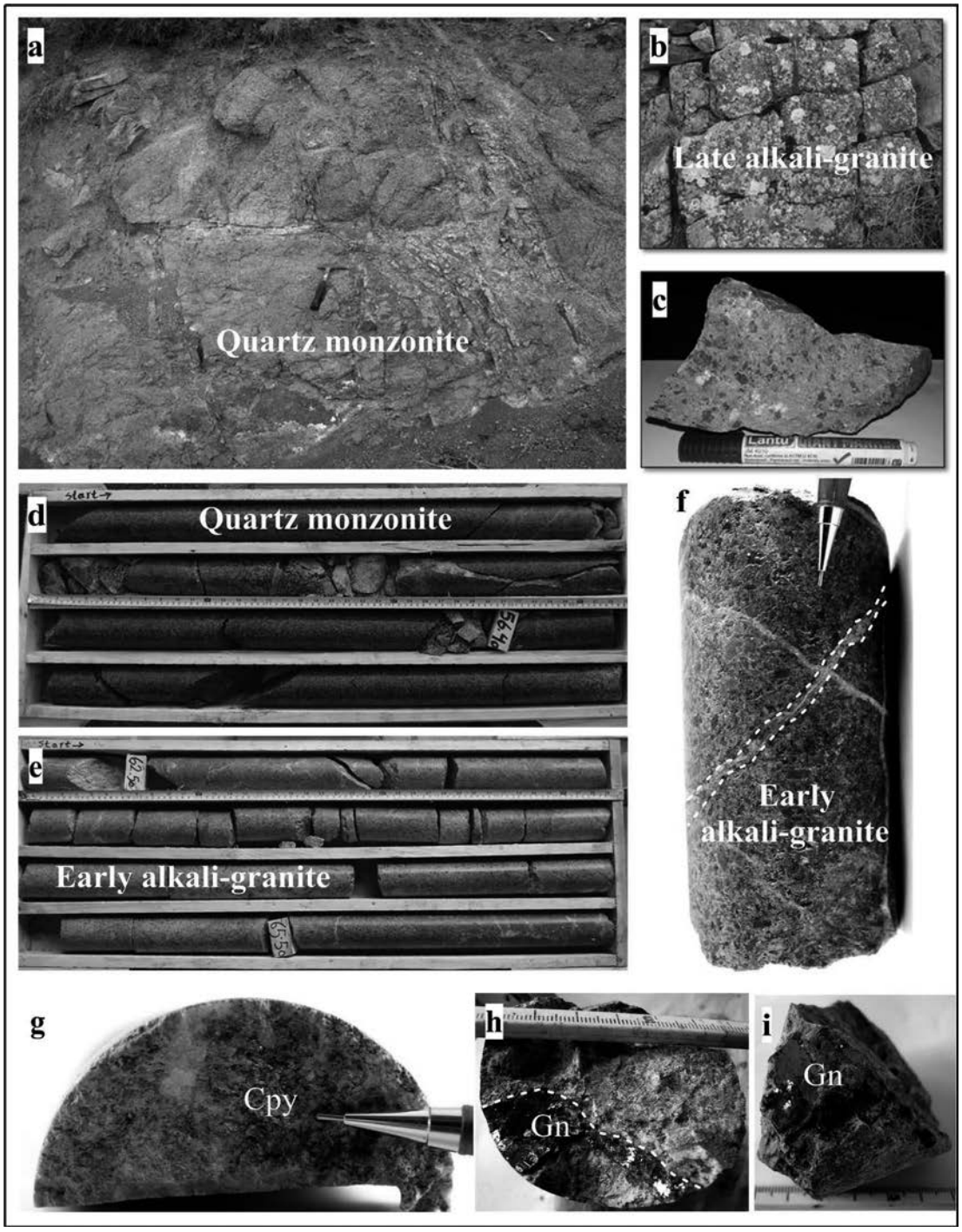

Fig. 2. a) Outcrop showing the ore-bearing quartz monzonite series which intruded the volcanic-volcaniclastic host rocks. b) Outcrop of late alkali-granite that postdating the quartz monzonite. c) Hand specimen of late alkali-granite from surface outcrop. d-e) Drill cores showing quartz monzonite and early alkali-granite samples of quartz monzonite to alkali-granite series. f) Ore bearing vein in the early alkali-granite from drill core samples. g-i) Ore bearing samples from drill cores. Mineral abbreviations: Cpy: Chalcopyrite; Gn: Galena.

were chosen after an initial petrographic study, then crushed, carefully hand-picked and separated using a binocular microscope. The purity of all concentrates was further checked by examination under a binocular microscope, to make sure that the concentrates, which were fresh, non-oxidized and contaminant-free, were essentially monomineralic. Sulfur isotope compositions of pyrite (n = 6), chalcopyrite (n = 6), sphalerite (n = 3) and galena (n = 3) were measured to better understand the physiochemical conditions of ore formation. Samples were

Table 1. $\delta^{34}S$ values of sulfide samples from the Chodarchay Cu-Au deposit.

Sample No.	Sample description	Depth (m)	Mineral	Texture	Stage	$\delta^{34}S$ (‰)
1-12	Alkali-granite	59.30	Sphalerite	veinlet	porphyry	2.0
1-12	Alkali-granite	59.30	Chalcopyrite	veinlet	porphyry	3.7
1-12	Alkali-granite	59.30	Galena	veinlet	porphyry	0.2
1-12	Alkali-granite	59.30	Pyrite	veinlet	porphyry	4.8
1-12b	Alkali-granite	59.30	Pyrite	veinlet	porphyry	4.6
2-2	Tuff	13.6	Chalcopyrite	clast	epithermal	3.3
2-2	Tuff	13.6	Pyrite	clast	epithermal	4.2
5-4	Breccia	35	Chalcopyrite	open space filling	epithermal	3.4
5-4	Breccia	35	Pyrite	open space filling	epithermal	3.8
7-1	Tuff	18	Galena	clast	epithermal	0.9
7-1	Tuff	18	Sphalerite	clast	epithermal	3.5
7-1	Tuff	18	Chalcopyrite	clast	epithermal	3.2
7-1	Tuff	18	Pyrite	clast	epithermal	4.9
7-1b	Tuff	18	Pyrite	clast	epithermal	5.0
7-3	Volcanic	37	Pyrite	breccia matrix	epithermal	5.1
7-3	Volcanic	37	Chalcopyrite	breccia matrix	epithermal	3.6
7-4	Volcanic	37.60	Sphalerite	veinlet	epithermal	0.9
15-16	Quartz monzonite	66.50	Galena	disseminated	porphyry	1.3
15-16	Quartz monzonite	66.50	Chalcopyrite	disseminated	porphyry	1.7
20-5	Alkali-granite	51.20	Pyrite	breccia	porphyry	6.8

analyzed by mass spectrometry using a Delta C Finnigan MAT continuous flow isotope-ratio mass spectrometer with an elemental analyzer, a TC-EA following the methodology of Giesemann et al. (1994). These analyses were carried out at the Centres Científicsi Tecnològics de la Universitat de Barcelona, Spain. The results are given as $\delta^{34}S$ ‰ values relative to the V-CDT (Vienna – Canyon del Diablo Troilite standard (V–CDT).

5. Results

5.1. Distribution of rock types

Magmatic and hydrothermal activity and related mineralization are recorded in the Chodarchay district. According to the existing rock units in the area, multiple phases of volcanic activity are thought to have occurred in the region. Relative temporal relationships of the units are established from observed contact relationships. The magmatic activity is divided into four classes: 1) The oldest outcropped Eocene lavas and volcaniclastics (Karaj Formation); 2) late Eocene-post Eocene quartz monzonite to alkali-granite; 3) late alkali-granite stock that cuts early intrusions (which has not been intersected by drilling); 4) Oligocene volcaniclastic units that contain lithics from the intrusions, these units may represent the final magmatic event in the deposit area. Volcanic and volcaniclastic units surround the intrusions.

Extrusive rocks: The oldest regional rocks are represented by the Karaj Formation volcanic and volcaniclastic units.

Rhyolite, andesite, trachyte and volcaniclastic units, mainly rhyolitic, outcrop in the area. The rhyolite has porphyry and porphyry-vitrophyre textures. Coarse crystals include plagioclase, alkali-feldspar and amphibole. Zircon is the accessory mineral in this rock. Trachyte has a porphyry texture. The phenocrystals include plagioclase, alkali-feldspar and quartz. Euhedral apatite is the accessory mineral in this rock. The andesitic volcanic unit is distal relative to the mining site. Volcaniclastic units seen in the Chodarchay are rhyolitic crystal- and lithic crystal-tuffs.

Intrusive rocks: The quartz monzonite unit at Chodarchay displays granular and graphic textures. The major minerals are euhedral to subhedral plagioclase, euhedral to anhedral orthoclase and anhedral quartz. Plagioclase shows polysynthetic twinning. Euhedral to subhedral amphibole (hornblende), euhedral clinopyroxene and subhedral biotite are the minor minerals. Magnetite is the predominant accessory phase. Other accessory minerals in this rock include euhedral apatite, euhedral zircon, titanite and disseminated ilmenite. Amphibole and biotite are replaced by chlorite. Plagioclase and orthoclase are replaced by sericite. The early alkali-granite shows granular and graphic textures. Major minerals consist of subhedral to anhedral orthoclase crystals. Anhedral to subhedral quartz is relatively large. Most quartz crystals show un-

dulose extinction. The plagioclase is euhedral and shows polysynthetic twinning. The biotite as a minor mineral is subhedral. The hornblende is euhedral to subhedral. Accessory minerals consist of subhedral to euhedral zircon, euhedral titanite and apatite that occur as inclusions inside the quartz and orthoclase. Late alkali-granite has porphyritic texture and consists of K-feldspar, plagioclase, quartz, amphibole and muscovite. Accessory minerals in these rocks include magnetite, ilmenite, titanite, apatite and zircon.

5.2. Distribution of mineralization

The mineralization at Chodarchay is hosted by quartz monzonite to alkali-granite series and extends into the Karaj Formation units. Epithermal mineralization is overprinted on porphyry mineralization at the Chodarchay deposit (Yasami et al. 2017). The Chodarchay sulfide mineralization system extends to the depth, and main ore minerals include chalcopyrite, pyrite, sphalerite, and galena. The high-sulfidation mineralization is followed by a late-stage supergene event with the deposition of secondary minerals such as chalcocite, digenite, and covellite. In summary, the mineralization (Fig. 2g–i) is associated with the quartz monzonite and Karaj Formation units and occurs as stockwork, veinlets, dissemination, open space filling and breccia ore in the stock and the surrounding volcanic-volcaniclastic rocks. The main sulfide minerals at the Chodarchay are chalcopyrite, pyrite with lesser sphalerite and galena. Chalcopyrite is the most abundant ore mineral at the Chodarchay deposit. Chalcopyrite occurs as fine-grained and disseminated crystals, veinlets and open space fillings. Chalcopyrite, sphalerite and galena in some parts from the epithermal stage have equilibrium boundaries that show they are contemporaneous. Pyrite is common in most altered and mineralized rocks. This mineral shows dissemination and veinlet textures. Sphalerite and galena exist in the quartz veinlets and mineralized breccias. In some parts, galena surrounds sphalerite indicating that galena formation continued after sphalerite (Fig. 3a–f). Enargite at the Chodarchay points to high-sulfidation epithermal mineralization. Tetrahedrite and tennantite sulfosalts occur as amorphous inclusions inside chalcopyrite and sphalerite. A summary of the paragenetic sequence is presented in Fig. 4. The paragenesis comprises two principal stages (porphyry and epithermal stages).

Alteration types are distributed in the rock units. Alteration, increasing in intensity towards mineralization, is zoned from proximal to distal. Quartz is the most abundant hydrothermal alteration mineral in the study area. Potassic alteration assemblage (secondary alkali-feldspar+secondarybiotite+magnetite+chalcopyrite) changes to phyllic alteration (quartz+sericite+pyrite) and then argil-

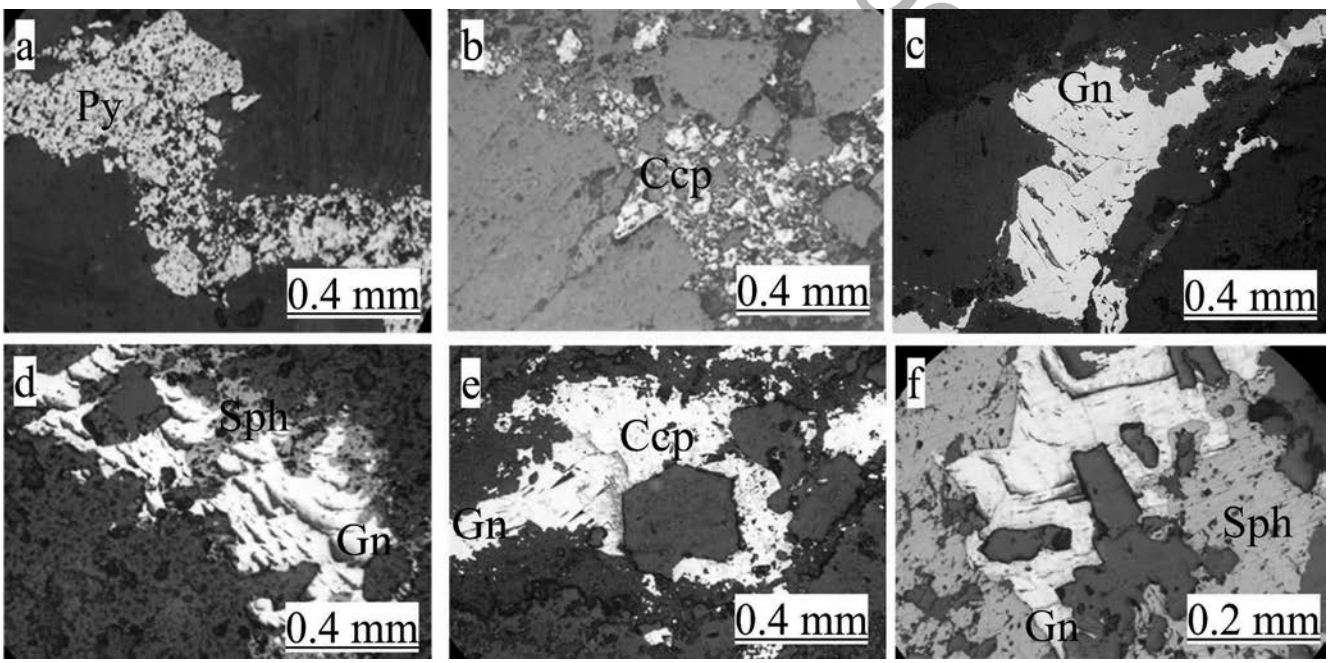

Fig. 3. Photomicrograph views showing main sulfide ore minerals (reflected light): a) Chalcopyrite (Cpy) within the quartz gangue. b) Co-precipitated sphalerite (Sph), galena (Gn) and chalcopyrite (Cpy) minerals. C) pyrite (py) crystals within the gangue. d) Sphalerite (Sph). e) Open space filling galena (Gn) and chalcopyrite (Cpy). f) sphalerite (Sph), galena (Gn) and chalcopyrite (Cpy); galena (Gn) surrounds sphalerite (Sph).

	Mineralization						
	Porphyry mineralization		Epithermal moneralization			Supergene	
Minerals	Stage 1	Stage 2	Stage 1	Stage 2	Stage 3	Stage 1	Stage2
Magnetite	—			—	—		
Hematite (Specularite)			—				
Pyrite	—	—	—	—	—		
Chalcopyrite	—		—	—			
Sphalerite		—		—			
Galena		—		—			
Tetrahedrite-Tenantite				—			
Enagite				—			
Gold				—			
Bornite				—	—		
Chalcosite				—	- - -	—	
Covellite				—	- - -	—	
Digenite				—	- - -	—	
Malachite							—
Azurite							—
Iron oxide							—

Fig. 4. Mineral association and paragenetic sequence of mineralization in the Chodarchay epithermal-porphyry deposit.

lic alteration (sericite, clay mineral, and quartz) or directly to the argillic alteration type at shallow depth. In the upper parts of the system, propylitic (chlorite and calcite or epidote) or argillic alteration occurs. Advanced argillic alteration (alunite, dickite, kaolinite and andalusite) overprints the early-formed alteration types. Mineralization and alteration show zonation from the porphyry system to the epithermal mineral assemblage.

5.3. $\delta^{34}S$ of sulfide ores

Sulfur isotope compositions for sulfides from the Chodarchay deposit are listed in Table 1. The $\delta^{34}S$ ratios of the ores range between +0.2 and +6.8 ‰, averaging 3.1 ‰, showing a pronounced Gaussian distribution (Fig. 5). The $\delta^{34}S$ values for pyrite (3.8 to 6.8 ‰), chalcopyrite (1.7 to 3.8 ‰), sphalerite (0.9 to 3.5 ‰) and galena (0.2 to 1.3 ‰) show a relatively narrow range.

The pyrite samples show trends to lower positive values with decreasing depth and temperature. The $\delta^{34}S$ in chalcopyrite is almost constant over the entire depth profile sampled. The number of galena and sphalerite samples is not enough for detailed interpretation. The sphalerite $\delta^{34}S$ pattern is much more widespread than the galena pattern. At a constant depth, pyrite has higher, and galena has lower $\delta^{34}S$ values. A local stratigraphic column for the Karaj Formation and late Eocene to post Eocene intrusion was provided by detailed petrography at the Chodarchay. The sequence of deposition is constrained by field mapping and core logging. Vertical distribution of sulfur isotopes for sulfide minerals and their host rocks at various depths of selected drill cores from the Chodarchay (as

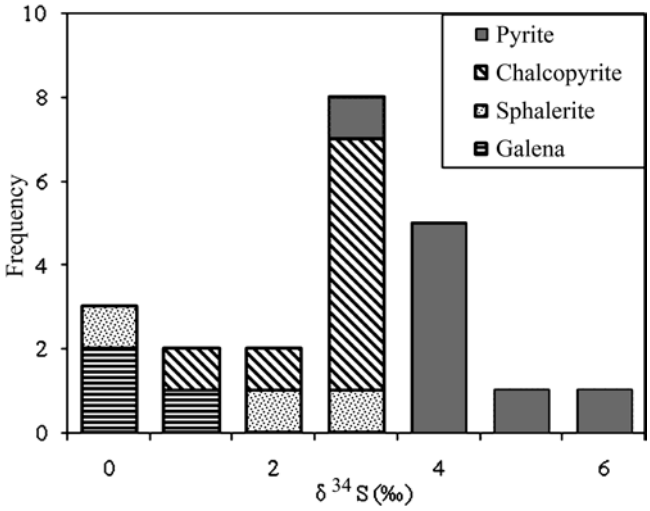

Fig. 5. Histogram of $\delta^{34}S$ values for sulfide minerals at the Chodarchay deposit.

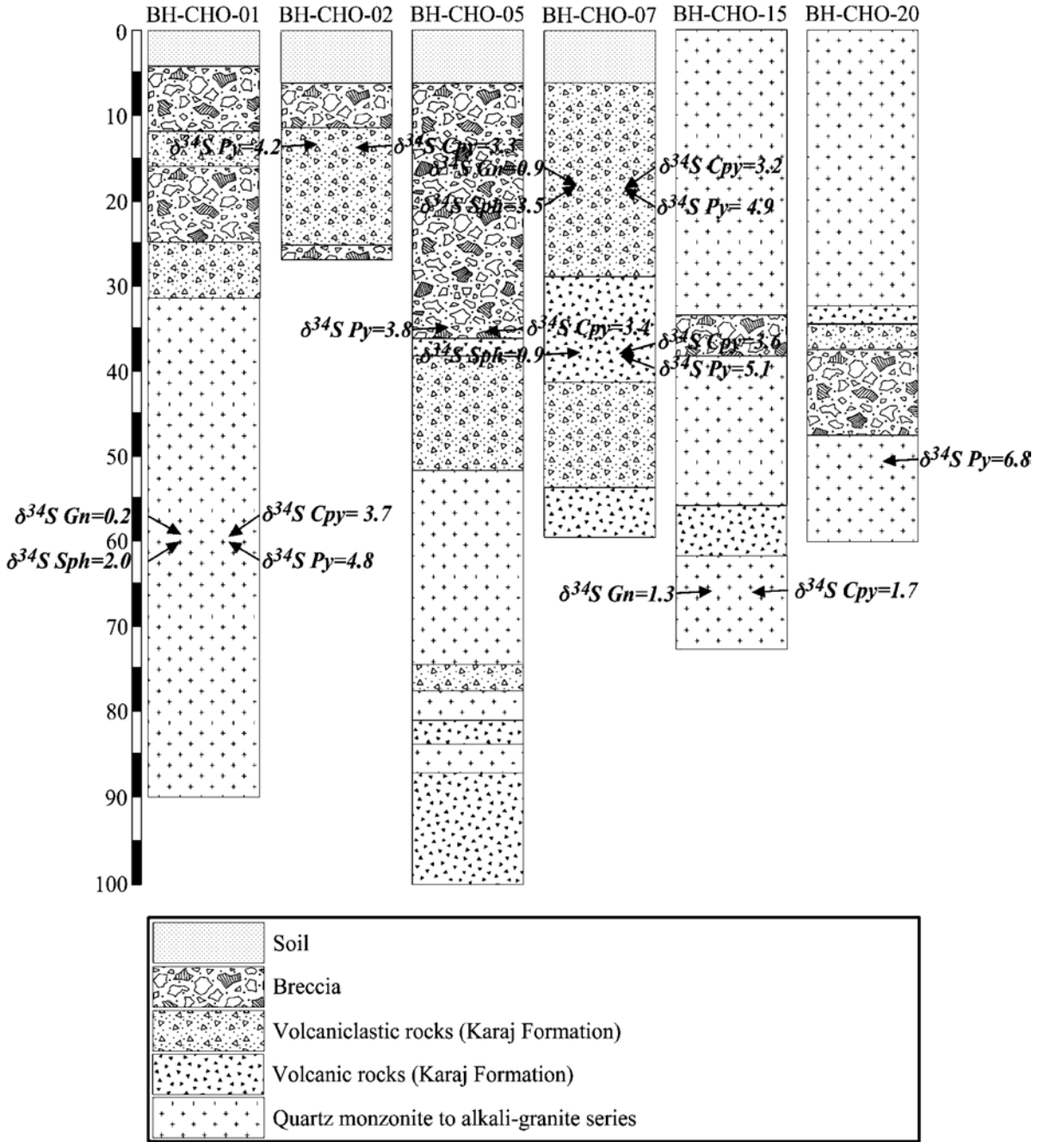

Fig. 6. Isotope compositions and rock units of selected drill cores from the Chodarchay deposit. Data and observations are based on the detailed petrographic and isotopic analysis of numerous specimens from BH-CHO-01, BH-CHO-02, BH-CHO-05, BH-CHO-07, BH-CHO-15 and BH-CHO-20 drill cores.

evidenced by core logging and petrography) is shown in Fig. 6.

6. Discussion

Although a number of studies during the past few years show that meteoric waters might play an important role in the formation of porphyry–epithermal systems (Taylor 1997, Simmons et al. 2005 and references therein), increasing evidence indicates an initial magmatic source for epithermal deposits (e.g. Giggenbach 1992, Vennemann et al. 1993, Kouzmanov et al. 2003).

Epithermal deposits occur in comparatively near-surface settings (< 1.5 km) and in general are strongly affected by magmatism, forasmuch as magmatism leads to

meteoric water distribution (Henley & Ellis1983, Taylor 2007). Magmatic volatiles and fluid boiling during pressure decrease are influential agents that control stable isotope attributes (Pirajno 2009). Epithermal deposits exhibit variable δD, $\delta^{18}O$, and $\delta^{34}S$ values (e.g. Hedenquist & Lowenstern 1994, Hedenquist 1997, Pirajno 2009) that show different contributions of meteoric water and magmatic water rich in volatiles and they are powerfully influenced by water/rock interaction with the surrounding rocks.

Relationships between porphyry mineralization and potassic alteration suggest that ore fluids had magmatic sources (e.g. Shahabpour & Kramers 1987). $\delta^{34}S$ sulfide values from PCDs are near 0‰, with lower (negative) $\delta^{34}S$ sulfide values typically related to deposition of sulfides from a sulfate-dominant (oxidized) fluid (Rye 1993, Wilson et al. 2007). Excursions to higher (positive) $\delta^{34}S$ sulfide values can be ascribed to changes in the bulk sulfur isotopic composition of the magma, either as a result of diverse contributions from the magmatic sulfur amount of sulfur extracted from the mantle, subduction zone fluids, seawater, or wall-rock assimilation (e.g. Sasaki et al. 1984, Vikre 2010). Sulfur isotope irregularities in porphyry and related deposits may reflect fluid interaction with wall rocks having varied $\delta^{34}S$ proportions in sulfide minerals, or are due to subsequent magmatic actions, such as degassing of SO_2 and following disproportionation to sulfide species.

While sulfides from magma should have isotopic compositions around 0‰, several deposits show distinctly negative $\delta^{34}S$ sulfide values (as do high-sulfidation epithermal Au deposits). Examples include the Dinkidi alkalic porphyry Cu–Au deposit, Philippines (Wolfe & Cooke 2011), the alkalic porphyry Cu–Au deposits of NSW, Australia (Heithersay & Walshe 1995, Wilson et al. 2007) and of British Columbia (Deyell & Tosdal 2005), and various calc-alkaline PCDs from Chile and the southwestern United States (e.g. Ohmoto & Rye 1979, Taylor 1987). Some of the elevated $\delta^{34}S$ sulfide values in the PCDs could represent a seawater sulfur contribution to the hydrothermal fluids (Sasaki et al. 1984).

$\delta^{34}S$ sulfide values from porphyry deposits are typically near 0‰, with lower (negative) $\delta^{34}S$ sulfide values typically related to deposition of sulfides from a sulfate-dominant (oxidized) fluid (e.g. Rye 1993, Wilson et al. 2007). Sulfur dioxide can disproportionate at temperatures around 350–450 °C, producing approximately 3 moles of SO_4 for every mole of H_2S (e.g. Rye et al. 1992, Rye 1993). If this process is the primary source of H_2S (aq) in PCDs, then sulfate should be the commanding type of aqueous sulfur in the mineralizing hydrothermal fluids. However, multiple paragenetic investigations have shown that sulfides are preponderant over sulfates in the altered rocks and ores (e.g. Wilson et al. 2003, Cannell et al. 2005, Seedorff et al. 2005, Vry et al. 2010). The excess SO_4^{2-} produced by SO_2 (g) disproportionation may flux to the near-surface environment. In exchange, inorganic sulfate reduction may take place in the porphyry environment, helping to generate additional H_2S needed to precipitate the considerable amount of bornite, chalcopyrite, and pyrite that characterize PCDs (e.g. Wilson et al. 2007).

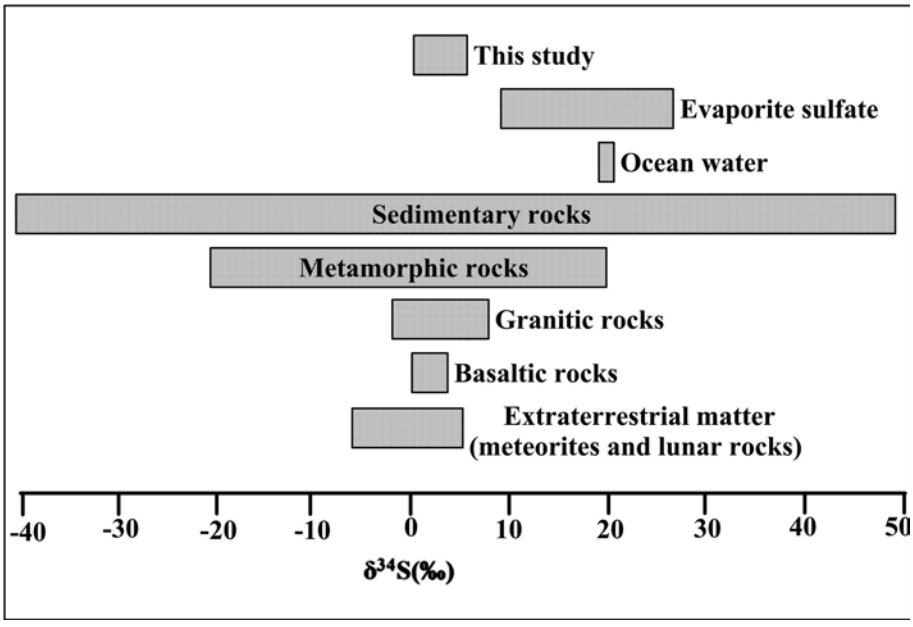

Fig. 7. $\delta^{34}S$ values for the Chodarchay deposit compared with those of geologically important sulfur reservoirs (Hoefs 2009).

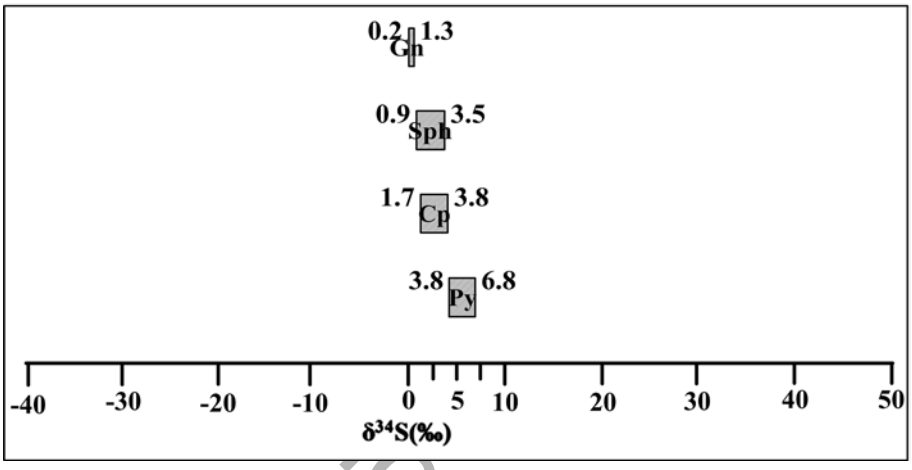

Fig. 8. Distribution of sulfur isotope composition of pyrite, chalcopyrite, galena and sphalerite of the mineralization related to the Chodarchay deposit. The values are expressed in permil, related to the standard VCDT (Vienna Canyon Diablo Troilite).

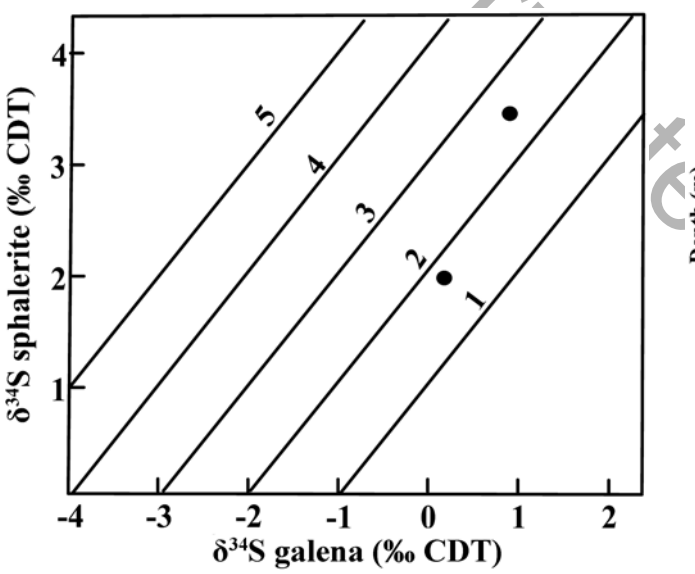

Fig. 9. Isotopic fractionation plot (after Ohmoto & Goldhaber 1997) with labeled sphalerite-galena fractionation as ‰. Numbers show relative partitioning of $\delta^{34}S$ between sphalerite and galena.

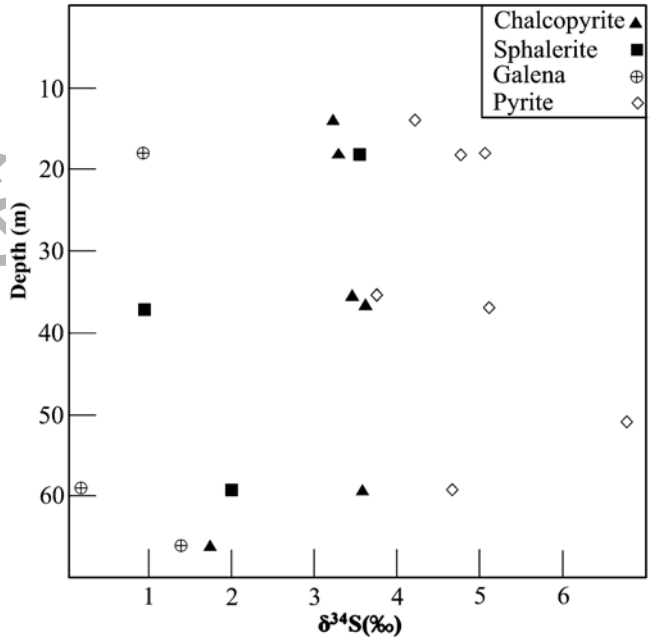

Fig. 10. Depth profile of $\delta^{34}S$ values for sulfide minerals from the Chodarchay deposit.

Compared with deposits like the Khalyfehlou in the southern part of Tarom where sulfur isotopes show negative values (−2.0 to −5.3 ‰) (Esmaeli et al. 2015), sulfur isotope values for the Chodarchay deposit in the northern part of Tarom are positive. The sulfur isotope values (0.2 to 6.8 ‰) for sulfides at the Chodarchay (Fig. 7) indicate a homogeneous magmatic source for the ore mineralization (Ohmoto 1979, Ohmoto & Goldhaber 1997) or a combination of magmatic and crustal origins (higher $\delta^{34}S$ values) (Pirajno & Bagas 2002, Hoefs 2009). Moreover, these data are similar to worldwide porphyry to epithermal deposits (Hedenquist & Lowenstern 1994, Ohmoto & Goldhaber 1997). The relative order of $\delta^{34}S$ enrichment is $\delta^{34}S$ pyrite > $\delta^{34}S$ chalcopyrite > $\delta^{34}S$ sphalerite > $\delta^{34}S$ galena (Fig. 8), suggesting sulfur isotope equilibrium in the mineralization stage (Ohmoto 1972, Alfonso et al. 2002, Hoefs 2009). The narrow range of sulfur isotopic values of the ores and the proximity of values to zero suggest a magmatic control on the mineralizing event and sourcing most of the sulfur from a magmatic system (Pirajno 2009). Sulfur isotopic compositions of hydrothermal ore minerals, with a characteristic decrease of $\delta^{34}S$ values through time are attributed to increasing oxidation of the fluids and sulfur isotope fractionation as a result of hydrolysis of magmatic SO_2 (Kouzmanov et al. 2003). Such isotopic compositions are consistent with similar

data sets from other high-sulfidation epithermal deposits (Arribas 1995) and are characteristically explained by sulfur isotope fractionation during hydrolysis of magmatically derived SO_2 and oxidation of fluid with decreasing temperature (Rye 1993). Geothermometric estimations for sulfur isotope fractionations of contemporaneous galena-sphalerite association at the Chodarchay, using the equation from Ohmoto & Rye (1979), give an equilibrium temperature close to 360 °C. This temperature belongs to an epithermal event. Temperatures obtained by sulfur isotope geothermometry at the Chodarchay deposit are typical as indicated by Arribas (1995) for the high-sulfidation epithermal systems. Measured $\delta^{34}S$ values for hydrothermal galena in the main mineralized zone are restricted to a narrow range (0.2 to 1.3 ‰) implying a homogeneous source. This range (0.2 to 1.3 ‰) can be explained to correlate with the range for volcanic SO_2. The sulfur isotope fractionation graph (Ohmoto & Goldhaber 1997) indicates sphalerite-galena fractionation of the mineralization varying around 2 ‰ (Fig. 9). They demonstrate a vertical $\delta^{34}S$ zonation consistent with the involvement of hydrothermal fluid (Fig. 10).

7. Conclusions

The Chodarchay is the first report of porphyry-epithermal mineralization along the Tarom subzone of western Alborz magmatic belt of NW Iran. There are several groups of rock units and alteration types in the area. Using observations from outcrops, core logging and petrography, quartz monzonite and its surrounding rock units are the host rocks to mineralization. Structural mapping emphasizes the role of the fault in mineralization along the deposit area.

Temperatures obtained by sulfur isotope geothermometry on samples from the epithermal part of the Chodarchay deposit are typical for high-sulfidation systems. Isotopic data for sulfide ore minerals from the deposit suggest a predominant magmatic origin for sulfur. Magma played a key role in supplying sulfur for ore mineralization at the deposit. Variations and decrease in $\delta^{34}S$ values are interpreted as sulfur isotope fractionation during hydrolysis of magmatic SO_2 and fluid oxidation through time with decreasing depth and temperature.

Acknowledgements

This paper is part of the first author's Ph.D. thesis at Tarbiat Modares University, Tehran, Iran. Appreciation is extended to Madankaran Angouran Company for generously providing field survey facilities and access to drill cores and exploration data. The Serveis Científico-Tècnics de la Universitat de Barcelona provided support for the sulfur isotope analyses and the Catalan Government's Department of Universities, Research and the Information Society provided assistance under research grant 2009SGR-00444 of the Departament d 'Universitats, Recercai Societat de la Informació (Generalitat de Catalunya). We would like to thank the three anonymous reviewers for their constructive reviews on an earlier version of the manuscript. Ralph Halama and Thomas Ulrich are also thanked for careful editorial handling of the manuscript.

References

Aghazadeh, M., Castro, A., Rashidnejad Omran, N., Emami, M. H., Moinvaziri, H. & Badrzadeh, Z. (2010): The gabbro (shoshonitic)–monzonite–granodiorite association of Khankandi pluton, Alborz Mountains, NW Iran. – J. Asian Earth Sci. **38**: 199–219.

Alfonso, P., Canet, C., Melgarejo, J. C. & Fallick, A. E. (2002): Sulphur isotope composition of Silurian shale-hosted PGE-Ag-Au-Zn-Cu mineralisations of the Prades Mountains (Catalonia, Spain). – Miner. Deposita **37**: 198–212.

Allen, M. B., Ghassemi, M. R., Shahrabi, M. & Qorashi, M. (2003): Accommodation of late Cenozoic shortening in the Alborz range, northern Iran. – J. Struct. Geo. **25**: 659–672.

Arribas, A. (1995): Characteristics of high-sulfidation epithermal deposits, and their relation to magmatic fluid. – In: Thompson, J. F. H. (ed.): Magmas, fluids and ore deposits. – Mineral. Assoc. Canada, Short Course Series **23**: 419–454.

Azizi, H. & Jahangiri, A. (2008): Cretaceous subduction-related volcanism in the northern Sanandaj-Sirjan Zone, Iran. – J. Geodyn. **45**: 178–190.

Berberian, M. (1983): The southern Caspian: a compressional depression floored by a trapped, modified oceanic crust. – Can. J. Earth Sci. **20**: 16–83.

Berberian, M. & King, G. C. P. (1981): Towards a paleogeography and tectonic evolution of Iran. – Can. J. Earth Sci. **18**: 210–265.

Bolourian, G. H. (1994): Petrology of the Tertiary Volcanic Rocks in the Northern Tehran. – M. Sc. thesis, Tarbiat Moallem University, Tehran, Iran (in Persian with English abstract), 145 pp.

Cannell, J. C., Cooke, D. R., Walshe, J. L. & Stein, H. (2005): Geology, mineralization, alteration, and structural evolution of the El Teniente porphyry Cu-Mo deposit. – Econ. Geol. **100**: 979–1003.

Deyell, C. & Tosdal, R. M. (2005): Sulfur isotopic zonation in BC alkalic porphyry Cu-Au systems: Applications to mineral exploration. – British Columbia and Yukon Chamber of Mines Mineral Exploration Roundup 2005, Abstract Volume, 29.

Esmaeli, M., Lotfi, M. & Nezafati, N. (2015): Fluid inclusion and stable isotope study of the Khalyfehlou copper deposit, southeast Zanjan, Iran. – Arab. J. Geosci. **8**: 9625–9633.

Field, C. W., Zhang, L., Dilles, J. H., Rye, R. O. & Reed, M. H. (2005): Sulfur and oxygen isotopic record in sulfate and sulfide minerals of early, deep, pre-main stage porphyry Cu–Mo and late main stage base-metal mineral deposits, Butte district, Montana. – Chem. Geol. **215**: 61–93.

Giesemann, A., Jaeger, H. J., Norman, A. L., Krouse, H. R. & Brand, W. A. (1994): Online sulfur-isotope determination using an elemental analyzer coupled to a mass spectrometer. – Anal. Chem. **66**: 2816–2819.

Giggenbach, W. F. (1992): SEG distinguished lecture: magma degassing and mineral deposition in hydrothermal systems along convergent plate boundaries. – Econ. Geol. **87**: 1927–1944.

Hashemi, A. G. & Taghipour, B. (2010): Advanced argillic alteration in Tarom zone, central Iran. – Goldschmidt Conference Abstracts.

Hassanzadeh, J., Ghazi, A. M., Axen, G. & Guest, B. (2002): Oligo-Miocene mafic alkaline magmatism north and northwest of Iran: evidence for the separation of the Alborz from the Urumieh-Dokhtar magmatic arc. – Geological Society of America Abstracts with Programs **34**: 331.

Hedenquist, J. W. (1997): Epithermal gold deposits: Styles, characteristics and exploration. – Key Centre Econ. Geol., Univ. West Aust., Short Course Notes.

Hedenquist, J. W. & Lowenstern, J. B. (1994): The role of magmas in the formation of hydrothermal ore deposits. – Nature **370**: 519–527.

Heithersay, P. S. & Walshe, Y. L. (1995): Endeavour 26 North: A porphyry copper-gold deposit in the Late Ordovician, shoshonitic Goonumbla volcanic complex, New South Wales, Australia. – Econ. Geol. **90**: 1506–1532.

Henley, R. W. & Ellis, A. J. (1983): Geothermal systems ancient and modern: A geochemical review. – Earth Sci. Rev. **19**: 1–50.

Hoefs, J. (2009): Stable Isotope Geochemistry. – 6th ed., Springer-Verlag, Berlin, 285 pp.

Hosseinzadeh, M. R., Maghfouri, S., Moayyed, M. & Rahmani, A. (2016): Khalifelu deposit: high sulfidation epithermal Cu-Au mineralization in the Tarom magmatic zone, north Khoramdareh. – Scientific Quarterly Journal of Geosciences **25**: 179–194.

John, D. A., Ayuso, R. A., Barton, M. D., Blakely, R. J., Bodnar, R. J., Dilles, J. H., Gray, F., Graybeal, F. T., Mars, J. C., Mcphee, D. K., Seal, R. R., Taylor, R. D. & Vikre, P. G. (2010): Porphyry copper deposit model, Chap. B of Mineral deposit models for resource assessment: U.S. Geological Survey Scientific Investigations Report 2010–5070–B, 169 pp.

Kouzmanov, K., Ramboz, C., Lerouge, C., Deloule, E., Beaufort, D. & Bogdanov, K. (2003): Stable isotopic constrains on the origin of epithermal Cu-Au and related porphyry copper mineralisation in the southern Panagyurishte district, Srednogorie zone, Bulgaria. – In: Elioupoulos, D. G. et al. (eds.): Mineral Exploration and Sustainable Development, Proceedings of the 7th biennial SGA meeting, Athens, Greece, 24-28 August 2003. A. A. Balkema Publishers: 1181–1184.

Mehrabi, B., Ghasemi Siani, M. & Azizi, H. (2016): The genesis of the epithermal gold mineralization at north Glojeh veins, NW Iran. – IJSBAR: 479–497.

Mirnejad, H., Hassanzadeh, J., Cousens, B. L. & Taylor, B. E. (2010): Geochemical evidence for deep mantle melting and lithospheric delamination as the origin of the inland Damavand volcanic rocks of northern Iran. – J. Volcanol. Geotherm. Res. **198**: 288–296.

Moayyed, M. (2001): Geochemistry and Petrology of Volcano-plutonic Bodies in Tarom Area. – Ph.D. thesis University of Tabriz, Iran (in Persian with English abstract), 256 pp.

Mokhtari, M. A. A., Kouhestani, H. & Saeedi, A. (2016): Investigation on type and origin of copper mineralization at Aliabad Mousavi-Khanchy occurrence, east of Zanjan, using petrological, mineralogical and geochemical data. – Scientific Quarterly Journal of Geosciences **25**: 259–270.

Nabatian, G. (2011): Geological map of the Tarom intrusive complex and adjacent areas, scale 1:25,000. – Tehran, Iran.

Nabatian, G. & Ghaderi, M. (2013): Oxygen isotope and fluid inclusion study of the Sorkhe-Dizaj iron oxide-apatite deposit, NW Iran. – Int. Geol. Rev. **55**: 397–410.

Nabatian, G., Ghaderi, M., Daliran, F. & Rashidnejad-Omran, N. (2013): Sorkhe-Dizaj iron oxide-apatite ore deposit in the Cenozoic Alborz–Azarbaijan magmatic belt, NW Iran. – Resour. Geol. **63**: 42–56.

Nabatian, G., Ghaderi, M., Corfu, F., Neubauer, F., Bernroider, M., Prokofiev, V. & Honarmand, M. (2014): Geology, alteration, age, and origin of iron oxide–apatite deposits in Upper Eocene quartz monzonite, Zanjan district, NW Iran. – Miner. Deposita **49**: 217–234.

Nazari, H. & Salamati, R. (1998): Roudbar 1:100,000, Geological map.

Ohmoto, H. (1972): Systematics of sulfur and carbon in hydrothermal ore deposits. – Econ. Geol. **67**: 551–579.

Ohmoto, H. (1979): Isotopes of sulfur and carbon. – In: Geochemistry of Hydrothermal Ore Deposits: 509–567.

Ohmoto, H. & Goldhaber, M. (1997): Sulfur and carbon isotopes. In: Barnes, H. L. (ed.): Geochemistry of Hydrothermal Ore Deposits, John Wiley and Sons, New York: 517–611.

Ohmoto, H. & Rye, R. O. (1979): Isotopes of sulfur and carbon. – In: Barnes, H. L. (ed.): Geochemistry of Hydrothermal Ore Deposits, 2nd ed., John Wiley and Sons, New York.

Pirajno, F. & Bagas, L. (2002): Gold and silver metallogeny of the South China Fold Belt: a consequence of multiple mineralizing events? – Ore Geol. Rev. **20**: 109–126.

Pirajno, F. (2009): hydrothermal process and mineral systems. – Springer, Geological Survey of Western Australia, Perth, WA, Australia, 1273 pp.

Qiu, L., Yan, D.-P., Tang, S.-L., Wang, Q., Yang, W.-X., Tang, X. & Wang, J. (2016): Mesozoic geology of southwestern China: Indosinian foreland overthrusting and subsequent deformation. – J. Asian Earth Sci. **122**: 91–105.

Rye, R. O. (1993): The evolution of magmatic fluids in the epithermal environment: the stable isotope perspective. – Econ. Geol. **88**: 733–752.

Rye, R. O. (2005): A review of the stable-isotope geochemistry of sulfate minerals in selected igneous environments and related hydrothermal systems. – Chem. Geol. **215**: 5–36.

Rye, R. O., Bethke, P. M. & Wasserman, M. D. (1992): The stable isotope geochemistry of acid sulfate alteration. – Econ. Geol. **87**: 225–262.

Sasaki, A., Ulrilsen, C. E., Sto, K. & Ishihara, S. (1984): Sulphur reconnaissance of porphyry copper and Manto-type deposits in Chile and the Philippines. – Bulletin of the Geological Survey of Japan **35**: 615–622.

Seedorff, E., Dilles, J. H. & Proffett, J. M. Jr. (2005): Porphyry deposits: Characteristics and origin of hypogene features. – Econ. Geol. **100**: 251–298.

Shahabpour, J. & Kramers, J. D. (1987): Lead isotope data from the Sar-Cheshmeh porphyry copper deposit, Iran. – Miner. Deposita **22**: 278–281.

Simmons, S. F., White, N. C. & John, D. A. (2005): Geological characteristics of epithermal precious and base metal deposits. – Econ. Geol. **100**: 485–522.

Taghipour, B. & Mackizadeh, M. A. (2010): Genesis of hydrothermal alteration using stable isotope geochemistry in Takestan area (Tarom zone). – J. Econ. Geol. **1**: 101–115 (in Persian with English abstract).

Taylor, B. E. (2007): Epithermal gold deposits. – In: Goodfellow, W. D. (ed.) Mineral Deposits of Canada: A Synthesis of Major Deposit-Types. District Metallogeny, the Evolution of Geological Provinces, and Exploration Methods, Special Publication **5**: 113–139. St. John's, NL: Geological Association of Canada, Mineral Deposits Division.

Taylor, E. M. (1987): Field geology of the northwest quarter of the Broken Top 15 quadrangle, Desch County, Oregon. Oregon Department of Geology and Mineral Industries. Special Paper **21**, 20 p., 1 map, scale 1:24,000.

Taylor, H. P. (1997): Oxygen and hydrogen isotope relationships in hydrothermal mineral deposits. – Geochemistry of Hydrothermal Ore Deposits, 3rd ed., 229–302.

Vennemann, T. W., Muntean, J. L., Kesler, S., Oneil, J. R., Valley, J. W. & Russell, N. (1993): Stable isotope evidence for magmatic fluids in the Pueblo-Viejo epithermal acid sulfate Au–Ag deposit, Dominican Republic. – Econ. Geol. **88**: 55–71.

Verdel, C., Wernicke, B. P., Hassanzadeh, J. & Guest, B. (2011): A Paleogene extensional arc flare-up in Iran. – Tectonics **30**: http://dx.doi.org/10.1029/2010TC002809 (TC3008)

Vry, J., Powell, R., Golden, K. M. & Petersen, K. (2010): The role of exhumation in metamorphic dehydration and fluid production. – Nat. Geosci. **3**: 31–35.

Wilson, A. J., Cooke, D. R. & Harper, B. J. (2003): The Ridgeway gold-copper deposit: A high-grade alkali porphyry deposit in the Lachlan fold belt, New South Wales, Australia. – Econ. Geol. **98**: 1637–1666.

Wilson, A. J., Cooke, D. R., Stein, H. J., Fanning, C. M., Holliday, J. R. & Tedder, I. J. (2007): U-Pb and Re-Os geochronologic evidence for two alkalic porphyry ore-forming events in the Cadia district, New South Wales, Australia. – Econ. Geol. **102**: 1–26.

Wolfe, R. C. & Cooke, D. R. (2011): Geology of the Didipio region and genesis of the Dinkidi alkalic porphyry Cu-Au deposit and related pegmatites, northern Luzon, Philippines. – Econ. Geol. **106**: 1279–1315.

Yasami, N., Ghaderi, M., Madanipour, S. & Taghilou, B. (2017): Structural control on overprinting high-sulfidation epithermal on porphyry mineralization in the Chodarchay deposit, northwestern Iran. – Ore Geol. Rev. **86**: 212–224.

Manuscript received: December 7, 2017
Revisions required: January, 31, 2018
Revised version received: February 13, 2018
Accepted: February 19, 2018
Responsible editor: Thomas Ulrich

Authors' addresses:

Narges Yasami, Department of Economic Geology, Tarbiat Modares University, Tehran 14115-175, Iran.

Majid Ghaderi (Corresponding author), Department of Economic Geology, Tarbiat Modares University, Tehran 14115-175, Iran.
E-mail: mghaderi@modares.ac.ir

Pura Alfonso, Dept. d'Enginyeria Minera, Industrial i TIC, Universitat Politécnica de Catalunya, Barcelona, Spain.